INTERNATIONAL JOURNAL OF
COASTAL, OFFSHORE & ENVIRONMENTAL ENGINEERING IJCOE Vol. 10 / No. 2 / Summer 2025 (16-34)

Available online at: www.ijcoe.org

Probability density functions of the DoB in tubular KT-joints of jacket-type platforms under out-of-plane bending loads

Hamid Ahmadi*[,1], Esmaeil Zavvar[2], Vahid Mayeli[3]

[1] *National Centre for Maritime Engineering and Hydrodynamics, Australian Maritime College (AMC), University of Tasmania, Launceston, TAS 7248, Australia.*

[2] *Department of Civil Engineering, Faculty of Engineering, University of Porto, Porto, Portugal.*

[3] *Faculty of Civil Engineering, University of Tabriz, Tabriz 5166616471, Iran.*

*Corresponding Author

E-mail Addresses: hamid.ahmadi@utas.edu.au (H. Ahmadi); esmaeilzavvar@gmail.com (E. Zavvar); mayeli.vahid@gmail.com (V. Mayeli)

ARTICLE INFO

Article History:
Received: 11 Mar 2024
Accepted: 03 Jul 2025

Keywords:
Tubular KT-joint; Fatigue; Degree of bending (DoB); Out-of-plane bending (OPB) moment loading; Probability density function (PDF); Weibull distribution; Kolmogorov-Smirnov test.

ABSTRACT

The degree of bending (DoB) has a profound effect on the fatigue behavior of tubular joints commonly found in offshore jacket structures. The DoB characterizes the through-the-thickness stress distribution and its value is essential for improving the accuracy of fatigue life estimation. Probability density functions (PDFs) of the random variables involved are necessary for the fatigue reliability analysis of jacket structures. The objective of present research was the derivation of PDF for the DoB in tubular KT-joints commonly found in jacket-type platforms. A total of 243 finite element (FE) analyses were carried out on 81 FE models of KT-joints subjected to three types of out-of-plane bending (OPB) moment loading. Generated FE models were validated using experimental data, previous FE results, and available parametric equations. Based on the results of parametric FE study, a sample database was prepared for the DoB values and density histograms were generated for respective samples based on the Freedman-Diaconis rule. Thirteen theoretical PDFs were fitted to the developed histograms, and the maximum likelihood (ML) method was applied to evaluate the parameters of fitted PDFs. In each case, the Kolmogorov-Smirnov test was used to evaluate the goodness of fit. Finally, the Weibull model was proposed as the governing probability distribution function for the DoB. After substituting the values of estimated parameters, six fully defined PDFs were presented for the DoB at the saddle positions of central and outer braces in KT-joints subjected to three types of OPB moment loading.

1. Introduction

Jacket-type offshore platforms widely used for oil/gas production primarily consist of circular hollow section (CHS) members, also called tubulars. The intersection among tubulars, in which the prepared ends of branch members (braces) are welded onto the undisturbed surface of a main member (chord), is called a tubular joint (Fig. 1). As a result of the formation and propagation of cracks due to wave-induced cyclic loads, tubular joints are susceptible to fatigue-induced damage during their service life.

One of the widely accepted approaches to estimate the fatigue life of a tubular joint is the stress-life (S-N) method that is based on the hot-spot stress (HSS) calculation. However, the study of many fatigue test results has shown that tubular joints of different geometry or loading type but with similar HSSs often exhibit significantly different numbers of cycles to failure [1]. Such differences are thought to be attributable to changes in crack growth rate that is dependent on the through-the-thickness stress distribution which can be characterized by the degree of bending (DoB) defined as the ratio of bending stress to total external stress.

Fig. 2 depicts the typical stress distribution through the chord wall of a tubular joint. Through-the-thickness stress field is a combination of the linear stress due to the chord wall bending and the nonlinear stress concentration at the weld toe due to the section change at the intersection. The nonlinear stress distribution around the weld toe is dependent on the weld geometry and is difficult to predict during the design stage. Since for a deep crack, the weld-toe stress concentration has a relatively little effect on the through-the-thickness stress field [2], the stress distribution across the wall thickness is usually assumed to be a linear combination of membrane and bending stresses. Hence, the DoB can be expressed as:

$$\mathrm{DoB} = \frac{\sigma_B}{\sigma_T} = \frac{\sigma_B}{\sigma_B + \sigma_M} \tag{1}$$

where σ_T is the total stress; and σ_B and σ_M are the bending and membrane stress components, respectively.

For the joints with low DoB, the standard stress-life approach may be unconservative. Hence, the current standard HSS-based S-N approach can be modified to include the effect of DoB in order to obtain more accurate fatigue life prediction. The other shortcoming of the S-N approach is that this method gives only the total life and can not be used to predict the fatigue crack growth and the remaining life of cracked joints. For the fatigue analysis of cracked joints, fracture mechanics (FM) should be used. The accurate determination of a stress intensity factor (SIF) is the key for FM calculations. Owing to the complexities introduced by the structural geometry and the nature of the local stress fields, it is impossible to calculate the SIFs analytically. This problem is often tackled by using simplified models, such as the flat plate solution and methods based on the T-Butt weight function with an appropriate load shedding model. To use these simplified SIF models to calculate the remaining fatigue life of tubular joints, the information is required again on the distribution of through-the-thickness stress acting on the anticipated crack path, which can be characterized by the DoB. Thus, DoB is an important input parameter for the calculation of fatigue crack growth in tubular welded joints.

Under any specific loading condition, the DoB value along the weld toe of a tubular joint is mainly determined by the joint geometry. To study the behavior of a tubular joint and to easily relate this behavior to the geometrical characteristics of the joint, a set of dimensionless geometrical parameters has been defined. Fig. 1 depicts a tubular KT-joint with the geometrical parameters τ, γ, β, α, and α_B for chord and brace diameters: D and d, and their corresponding wall thicknesses: T and t, and lengths: L and l. Critical positions along the weld toe of the central and outer braces for the calculation of the DoB values in a tubular joint, i.e. saddle, crown, toe, and heel have been shown in Fig. 1.

Since 1990s, a few research works has been devoted to the study of the DoB in simple tubular connections such as X- and K-joints. However, for tubular joints with complex geometry such as KT-joints which are quite common in offshore structures, the DoB has not been comprehensively investigated.

In a deterministic fatigue analysis, limiting assumptions should be made on numerous input parameters some of which exhibit considerable scatter. Consequently, deterministic analyses usually result in conservative designs. This fact emphasizes the significance of reliability-based fatigue analysis and design methods in which the key parameters of the problem can be modeled as random variables. The fundamentals of fatigue reliability assessment, if properly applied, can provide immense insight into the fatigue performance and safety of the structural system. Regardless of the method used for the reliability-based fatigue analysis and design of offshore structures, the probabilistic and statistical measures of the DoB are required as input parameters. DoB shows considerable scatter highlighting the significance of deriving its governing probability distribution function.

In the present research, initially, available literature on the DoB was surveyed (Sect. 2). Afterwards, a total of 243 finite element (FE) analyses were carried out on 81 FE models of tubular KT-joints which are among the most common joint types in jacket-type oil/gas production platforms. FE analyses were conducted under three types of out-of-plane bending (OPB) loads as shown in Fig. 3. Generated FE models were validated using the existing experimental data, FE results, and parametric equations. Based on a parametric FE investigation, a sample database was created for the DoB (Sect. 3); and density histograms were generated for respective samples (Sect. 4). Thirteen theoretical PDFs were fitted to the developed histograms, and the maximum likelihood (ML) method was applied to evaluate the parameters of fitted PDFs (Sect. 5). In each case, the Kolmogorov-Smirnov test was used to assess the goodness of fit (Sect. 6). Finally, a probability distribution model was proposed for the DoB; and after substituting the values of estimated parameters, six fully defined PDFs were presented for the DoB at the saddle positions of the central and outer braces in tubular KT-joints subjected to three types of OPB moment loading (Sect. 7).

2. Literature survey

2.1. Deterministic analysis of the DoB

Morgan and Lee [3] derived mean and design equations for DoB values at critical positions in axially loaded tubular K-joints from a previously established FE database of 254 joints. Design equations met all the acceptance criteria recommended by the UK DoE [4].

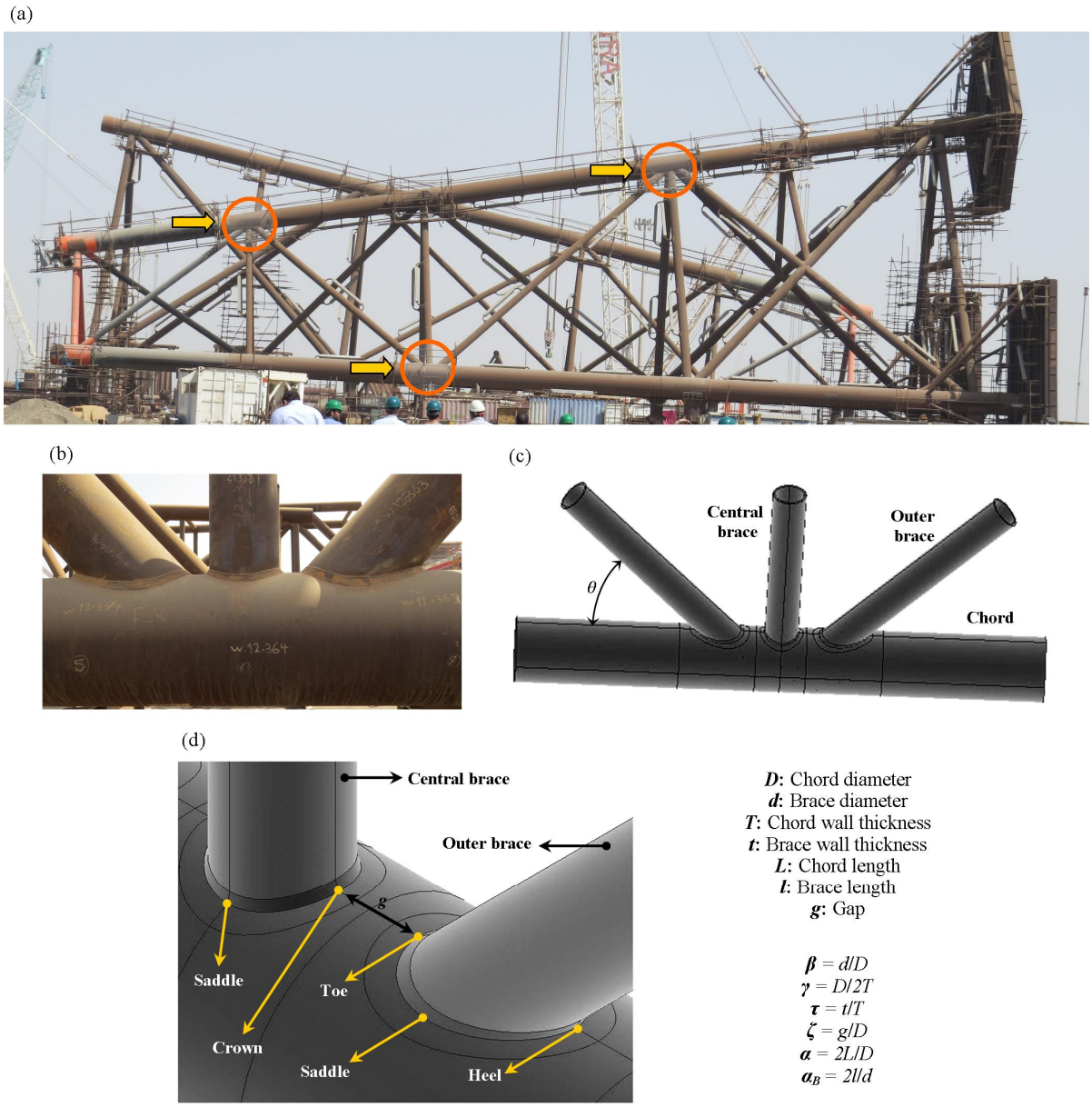

Fig. 1. (a) Tubular KT-joints in a jacket structure during the fabrication, (b) Close view of a welded tubular KT-joint, (c) Geometrical notation for a tubular KT-joint, (d) Critical positions along the weld toe of central and outer braces

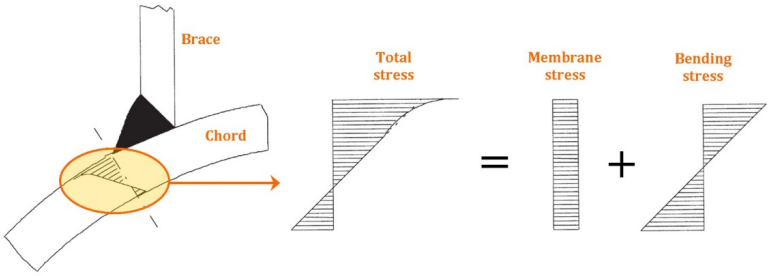

Fig. 2. Through-the-thickness stress distribution in a tubular joint

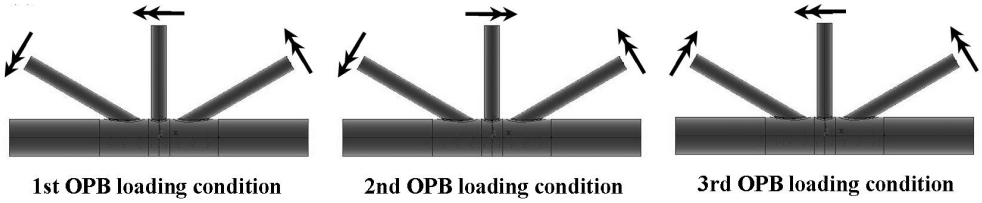

Fig. 3. Three applied OPB moment loading conditions

Chang and Dover [2] carried out a series of systematic thin-shell FE analyses for 330 tubular X- and DT-joints typically found in offshore structures under six different types of loading. Based on the results of nearly 2000 FE analyses, a set of parametric equations was developed to calculate the DoB at critical positions. Lee and Bowness [5] proposed an engineering methodology for estimating SIF solutions for semi-elliptical weld-toe cracks in tubular joints. The methodology uses the T-butt solutions proposed previously by the authors in conjunction with the stress concentration factors (SCFs) and the DoB values in uncracked tubular joints. Shen and Choo [6] determined the SIFs for a grouted tubular joint. They found that the fatigue strength of a grouted joint may be lower than that of as-welded joint, because when normalized with the HSS, the shape factor of grouted joint is higher than that of original as-welded joint due to the reduction in the DoB caused by the presence of in-filled grout in the chord. For grouted tubular joints, it is essential to consider the effect of DoB in practical fatigue assessment using HSS approach.

Ahmadi et al. [7] performed a set of parametric stress analyses on 81 K-joint FE models subjected to two different types of in-plane bending (IPB) loads. Analysis results were used to present general remarks on the effect of geometrical parameters on the DoB values at the toe and heel positions; and a new set of DoB parametric equations was developed. Ahmadi and Asoodeh [8] analyzed 81 K-joint FE models subjected to two types of OPB loading. Results were used to study the geometrical effects on the DoB at the saddle position; and two new DoB design formulas were proposed. Ahmadi and Asoodeh [9] studied the DoB in uniplanar tubular KT-joints subjected to axial loads. Their study was limited to the central brace DoB values and no design equation was proposed for the DoB along the weld toe of the outer braces. Also, IPB and OPB loadings were not included. Ahmadi and Amini Niaki [10] studied the degree of bending in two-planar tubular DT-joints under axial and bending loads. They developed a set of parametric equations to predict the DoB values at the saddle and crown positions.

2.2. Probabilistic analysis of the DoB

Ahmadi and Ghaffari [11] proposed a set of probability density functions for the DoB in tubular X-joints subjected to bending loads. Ahmadi and Ghaffari [12] developed probability distribution models for the DoB and SIF values in axially loaded tubular K-joints.

2.3. Remarks

Based on the above discussion, it is concluded that:

1. Despite the comprehensive research carried out on the study of SCFs and SIFs in tubular joints (e.g. [13-24] for SCFs, and [25, 26] for SIFs, among many others), the research works on the DoB in tubular joints are scarce and the studied joint types are limited to simple connections. Although tubular KT-joints are commonly found in steel offshore structures, the DoB in such joints has not been comprehensively investigated.
2. Results of research work reported in the literature are mostly suitable for deterministic analyses; and probabilistic studies are only limited to K- and X-joints. No probabilistic investigation has been carried out on the DoB of KT-joints; and there is no probability density function available for the DoB values to be used in reliability-based fatigue analysis and design of this type of joint.

3. Preparation of the DoB sample database

3.1. Details of FE modeling and analysis

FE-based software package ANSYS Ver. 11 was used in the present research for the FE modeling and analysis of tubular KT-joints subjected to OPB loadings in order to extract the DoB values for the probabilistic study.

3.1.1. Modeling of the weld profile

Accurate modeling of the weld profile is one of the important factors affecting the accuracy of the DoB results. In the present research, the welding size along the brace-to-chord intersection satisfies the AWS D 1.1 [27] specifications. The weld sizes at the crown, saddle, toe, and heel positions can be determined as follows:

$$H_w(\text{mm}) = 0.85t(\text{mm}) + 4.24$$

$$L_w = \frac{t}{2}\left[\frac{135^\circ - \psi\ (\text{deg.})}{45^\circ}\right]$$

$$\psi = \begin{cases} 90^\circ & \text{Crown} \\ 180^\circ - \cos^{-1}\beta\ (\text{deg.}) & \text{Saddle} \\ 180^\circ - \theta\ (\text{deg.}) & \text{Toe} \\ \theta\ (\text{deg.}) & \text{Heel} \end{cases} \quad (2)$$

The parameters used in Eq. (2) are defined in Fig. 4. As an example, the weld profiles generated for the central and outer braces of the joint model SKTJ1 (α = 16, α_B = 8, ζ = 0.3, τ = 0.4, β = 0.4, γ = 12, θ = 30˚) are shown in Fig. 5. For details of the weld profile modeling according to AWS D 1.1 [27], the reader is referred to Lie et al. [28] and Ahmadi et al. [29].

3.1.2. Definition of boundary conditions

The chord end fixity conditions in offshore tubular joints may range from almost fixed to almost pinned with generally being closer to almost fixed [30]. In practice, the value of the parameter α in over 60% of tubular joints is more than 20 and it is bigger than 40 in 35% of the joints [31]. Changing the end restraint from

fixed to pinned results in a maximum increase of 15% in the HSS at crown position for the joints with $\alpha = 6$; and this increase reduces to only 8% for $\alpha = 8$ [3]. In the view of the fact that the effect of chord end restraints is only significant for joints with $\alpha < 8$ and high β and γ values, which do not commonly occur in practice, both chord ends were assumed to be fixed, with the corresponding nodes restrained.

Under each of the three considered loading conditions, only an appropriate portion of the entire tubular KT-joint is required to be modeled. The reason is the symmetry in geometry, material properties, and chord-end boundary conditions of the joint, as well as loading symmetry/antisymmetry. This allowed us to consider a reduced FE problem instead of the actual one. Thus, the order of the global stiffness matrix and total number of stiffness equations were reduced, and computer solution time was substantially decreased. Table 1 and Fig. 6 describe the required portion to be modeled for each load case. Appropriate symmetric/antisymmetric boundary conditions were defined for the nodes located on the symmetry/antisymmetry planes.

3.1.3. Generation of the FE mesh

ANSYS element type SOLID95 was used in present research to model the chord, braces, and the weld profiles. These elements have compatible displacements and are well-suited to model curved boundaries. The element is defined by 20 nodes having three degrees of freedom per node and may have any spatial orientation. Using this type of 3-D brick elements, the weld profile can be modeled as a sharp notch. This method will produce more accurate and detailed stress distribution near the intersection in comparison with a shell analysis.

To guarantee the mesh quality, a sub-zone mesh generation method was used during the FE modeling. In this method, the tubular KT-joint was divided into several sub-zones according to computational requirements. The mesh of each sub-zone was then generated separately, and the meshing of the joint was finally completed by merging the meshes of the sub-zones. Quality and quantity of the mesh can be feasibly controlled by this method, and badly distorted elements can be avoided. The mesh generated by this method for a tubular KT-joint is shown in Fig. 7.

In the present paper, nodal stresses were used to extract the HSSs. When ANSYS solves stress, it does so on an element-by-element basis. Unless otherwise prompted, ANSYS will solve for the stresses at the Gauss points and extrapolate to the nodes. However, many elements share nodes. Thus, ANSYS averages the nodal stresses computed from each of the adjacent elements. If the mesh is sufficiently small, the averaged stresses will not be very different from the un-averaged stresses. In fact, there will be no big difference among stresses at a common node computed from adjacent elements. Hence, if one observes in the plot of un-averaged stresses that the stress changes drastically from a specific element to the next one, the generated mesh is not small enough. In the present research, the mesh generated for the critical zones such as the extrapolation region was sufficiently fine to avoid such problems.

It is explained in Sect. 3.1.4 that the geometric stresses perpendicular to the weld toe are required to be calculated to determine the DoB at the weld toe position based on Eq. (1). As shown in Fig. 8a, to extract the geometric stresses perpendicular to the weld toe, the region near the weld toe was meshed finely. The width of this region is discussed in Sect. 3.1.4.

To make sure that the results of the FE analysis are not affected by the inadequate quality or the size of the generated mesh, convergence test was conducted and meshes with different densities were used in this test, before generating the 81 models. Based on the results of convergence test, the number of elements through the chord and brace thickness was 2 (Fig. 8b); the number of elements on the surface, base, and back of the weld profile was 2 (Fig. 8c); the number of elements along the ½ of entire brace-to-chord intersection was selected to be 10 and 15 for the central and outer braces, respectively (Fig. 8d); and the number of elements inside the extrapolation region was selected to be 16 (Fig. 8a).

3.1.4. Analysis and extraction of DoB values

To obtain the DoB values in a tubular joint, static analysis of the linearly elastic type is suitable. The Young's modulus and Poisson's ratio were taken to be 207 GPa and 0.3, respectively.

To determine the weld-toe DoB values, according to Eq. (1), bending and membrane stress components should be known. These components can be calculated as follows:

$$\sigma_B = \frac{\sigma_O - \sigma_I}{2} \tag{3}$$

$$\sigma_M = \frac{\sigma_O + \sigma_I}{2} \tag{4}$$

where σ_O and σ_I are the hot-spot stresses (HSSs) at the weld toe on the outer and inner surfaces of the chord, respectively.

Eqs. (1), (3), and (4) lead to the following relation for the DoB based on the HSSs:

$$\mathrm{DoB} = \frac{1}{2}\left(1 - \frac{\sigma_I}{\sigma_O}\right) \tag{5}$$

To determine the HSSs, the stress at the weld-toe position should be extracted from the stress field outside the region influenced by the local weld-toe geometry. The location from which the stresses have to be extrapolated, called extrapolation region, depends

on the dimensions of the joint and on the position along the intersection. According to the recommendations of IIW-XV-E [32], the first extrapolation point should be at a distance of 0.4T from the weld toe, and the second point must be 1.0T further from the first point (Fig. 9a). The HSS is obtained by the linear extrapolation of the geometric stresses at these two points to the weld toe.

To extract and extrapolate the stresses perpendicular to the weld toe, as shown in Fig. 8a, the region between the weld toe and the second extrapolation point was meshed in such a way that each extrapolation point was placed between two nodes located in its immediate vicinity. These nodes are located on the element-generated lines which are perpendicular to the weld toe ($X_\perp$ direction in Fig. 9b).

At an arbitrary node inside the extrapolation region, the stress component in the direction perpendicular to the weld toe can be calculated, through the transformation of primary stresses in the global coordinate system, using the following equation:

$$\sigma_{\perp N} = \sigma_x l_1^{\,2} + \sigma_y m_1^{\,2} + \sigma_z n_1^{\,2} + 2\left(\tau_{xy} l_1 m_1 + \tau_{yz} m_1 n_1 + \tau_{zx} n_1 l_1\right) \tag{6}$$

where σ_a and τ_{ab} ($a, b = x, y, z$) are components of the stress tensor which can be extracted from ANSYS analysis results; and l_1, m_1, and n_1 are transformation components.

At the saddle, crown, toe, and heel positions, Eq. (6) is simplified as:

$$\sigma_{\perp N} = \sigma_x l_1^{\,2} + \sigma_y m_1^{\,2} + 2\tau_{xy} l_1 m_1 \quad \text{(Saddle)} \quad ;$$
$$\sigma_{\perp N} = \sigma_z \quad \text{(Crown, Toe, and Heel)} \tag{7}$$

Transformation components can be obtained as follows:

$$l_1 = \cos\left(X_\perp, x\right) = \left(x_w - x_n\right)/\delta \;;$$
$$m_1 = \cos\left(X_\perp, y\right) = \left(y_w - y_n\right)/\delta \tag{8}$$

$$\delta = \sqrt{\left(x_w - x_n\right)^2 + \left(y_w - y_n\right)^2 + \left(z_w - z_n\right)^2} \tag{9}$$

where $X_\perp$ is the direction perpendicular to the weld toe (Fig. 9b); x, y, and z are the axes of global Cartesian coordinate system; (x_n, y_n, z_n) and (x_w, y_w, z_w) are coordinates of the considered node inside the extrapolation region and its corresponding node at the weld toe position, respectively; and δ is the distance between the weld toe and the considered node inside the extrapolation region.

Stress at an extrapolation point is obtained as follows:

$$\sigma_{\perp E} = \frac{\sigma_{\perp N1} - \sigma_{\perp N2}}{\delta_1 - \delta_2}\left(\Delta - \delta_2\right) + \sigma_{\perp N2} \tag{10}$$

where $\sigma_{\perp Ni}$ (i = 1 and 2) is the nodal stress in the immediate vicinity of the extrapolation point in a direction perpendicular to the weld toe (Eq. (7)); δ_i (i = 1 and 2) is obtained by Eq. (9); and Δ equals to 0.4T and 1.4T for the first and second extrapolation points, respectively (Fig. 9b).

The extrapolated stress at the weld toe position, HSS, is calculated by the following equation:

$$\sigma_{\perp W} = 1.4\sigma_{\perp E1} - 0.4\sigma_{\perp E2} \tag{11}$$

where $\sigma_{\perp E1}$ and $\sigma_{\perp E2}$ are the stresses at the first and second extrapolation points in the direction perpendicular to the weld toe, respectively (Eq. (10)).

If the considered nodes in the calculations of Eqs. (7)–(11) are located on the outer surface of the chord, the value of $\sigma_{\perp W}$ obtained from Eq. (11) is used as σ_O in Eq. (5); and if the considered nodes are located on the inner surface of the chord, the result of Eq. (11) is equivalent to σ_I which is required for the calculation of the DoB in Eq. (5).

To facilitate the calculation of DoB values, above formulation was implemented in a macro file developed by the ANSYS parametric design language (APDL). The input data required to be provided by the user of the macro file are the chord thickness, label number of the node located at the weld toe, and the label numbers of the nodes inside the extrapolation region. These nodes can be introduced using the graphic user interface (GUI).

3.1.5. Verification of the FE modeling

As far as the authors can tell, there is no experimental data available in the literature on the DoB values in tubular KT-joints. However, previous research works offer some experimental data, FE results, and parametric equations that can be used to validate the FE model developed in the present study.

3.1.5.a. Comparison with HSS experimental data

According to Eq. (5), DoB is a function of σ_O and σ_I that are the HSSs at the weld toe on the outer and inner surfaces of the chord, respectively. Hence, if the proposed FE model could predict the HSS accurately, then undoubtedly it can result in accurate DoB values.

To verify the developed FE modeling procedure, a validation FE model was generated, and its results were compared with the results of experimental tests carried out by the first author on a KT-joint (Figs. 10 and 11). Details of the test setup and program presented by Ahmadi [33] are not repeated here for the sake of brevity. Results of verification process are presented in Table 2. There is good agreement between the results of present FE model and experimental data; and the average difference is about 10%. Hence, the developed FE models can be considered accurate enough to provide valid results.

Table 1. Appropriate portion of an entire tubular KT-joint required to be modeled for each load case

Load case (Fig. 3)	Required portion to be modeled
1st OPB moment loading condition	¼ (Fig. 6b)
2nd OPB moment loading condition	¼ (Fig. 6b)
3rd OPB moment loading condition	½ (Fig. 6a)

Table 2. Results of FE model verification based on experimental data

Loading	Position	HSS value of the chord's outer surface (σ_O)		Difference
		Present FE model	Experimental test [33]	
Axial	Saddle	5.48e+6	5.89e+6	6.96%
	Crown	2.94e+6	3.38e+6	13.02%

Table 3. Geometrical properties of the tubular K-joint specimen used for the verification of FE models

Loading	Joint ID	D (mm)	τ	β	γ	α	θ	ζ
Axial	JISSP 3.3 [34]	508	1.0	0.5	20.3	12.6	45˚	0.15
IPB	KJ-1 [7]	500	0.4	0.4	12.0	12.0	30˚	0.15
OPB	KJ-1 [8]	500	0.4	0.4	12.0	12.0	30˚	0.15

Table 4. Results of the FE model verification based on available parametric equations/FE results

Loading	Position	DoB values		Difference
		Present FE model	Available data	
Axial (Fig. 12a)	Saddle	0.6666	0.5529 (Morgan and Lee [3] Eq. (3d))	20.56%
	Toe	0.8727	0.8989 (Morgan and Lee [3] Eq. (3f))	2.91%
	Heel	0.7728	0.6997 (Morgan and Lee [3] Eq. (3b))	10.45%
IPB (Fig. 12b)	Toe	0.5991	0.5742 (Ahmadi et al. [7] FE model)	4.16%
OPB (Fig. 12c)	Saddle	0.8920	0.8045 (Ahmadi and Asoodeh [8] FE model)	10.87%

Table 5. Values assigned to each dimensionless parameter

Parameter	Definition	Value(s)
β	d/D	0.4, 0.5, 0.6
γ	$D/2T$	12, 18, 24
τ	t/T	0.4, 0.7, 1.0
θ		30˚, 45˚, 60˚
ζ	g/D	0.3
α	$2L/D$	16
α_B	$2l/d$	8

Table 6. Statistical measures of the generated DoB samples at the saddle positions of central and outer braces under the OPB loadings (LC: loading condition)

Statistical measure	DoB samples					
	Sample 1	Sample 2	Sample 3	Sample 4	Sample 5	Sample 6
	Central brace, 1st OPB LC	Central brace, 2nd OPB LC	Central brace, 3rd OPB LC	Outer brace, 1st OPB LC	Outer brace, 2nd OPB LC	Outer brace, 3rd OPB LC
n	81	81	81	81	81	81
μ	0.7677	0.7554	0.8031	0.7300	0.7672	0.7112
σ	0.0406	0.0534	0.0406	0.0858	0.0684	0.0774
α_3	-0.2557	-0.5833	-0.3283	0.5302	-0.9654	-0.2877
α_4	2.4892	2.7189	2.2563	1.5652	4.0385	1.9325

3.1.5.b. Comparison with available DoB parametric equations and FE results

A set of FE parametric studies have been conducted by Morgan and Lee [3], Ahmadi et al. [7], and Ahmadi and Asoodeh [8] for the prediction of DoB values in tubular K-joints under the axial, IPB, and OPB loadings, respectively. Results of these studies were used in present research to validate the developed FE model. To so, three K-joint FE models were generated having typical geometrical characteristics (Table 3) and they were analyzed under the axial, IPB, and OPB loadings shown in Fig. 12. Geometrical properties of the axially-loaded FE model were selected based on the data provided by HSE OTH 354 [34] for a steel specimen tested to determine the SCFs; and geometrical properties of the IPB- and OPB-loaded FE

models were selected in accordance with the validity range of the FE study conducted by Ahmadi et al. [7] and Ahmadi and Asoodeh [8].

The method of geometrical modeling (introducing the chord, braces, and weld profiles), the mesh generation procedure (including the selection of element type and size), analysis method, and the method of DoB extraction are identical for the validating models and the KT-joint models used for parametric study. Hence, the verification of DoB values derived from validating FE models with the results of equations proposed by Morgan and Lee [3], FE results of Ahmadi et al. [7], and FE results of Ahmadi and Asoodeh [8] lends support to the validity of DoB values derived from the KT-joint FE models.

Results of verification process are presented in Table 4. It can be seen that there is a good agreement among the results of present FE model and equations proposed by Morgan and Lee [3], FE results of Ahmadi et al. [7], and FE results of Ahmadi and Asoodeh [8]. The average difference is less than 10%. Hence, the generated FE models can be considered to be accurate enough to provide valid results.

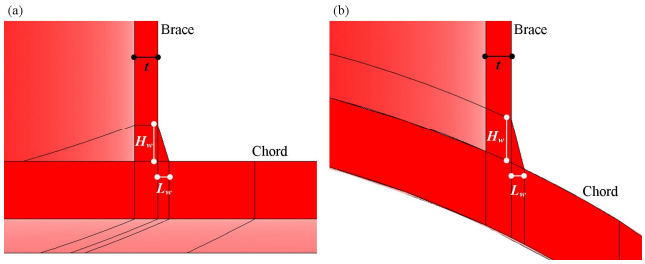

Fig. 4. Weld dimensions: (a) Crown position, (b) Saddle position

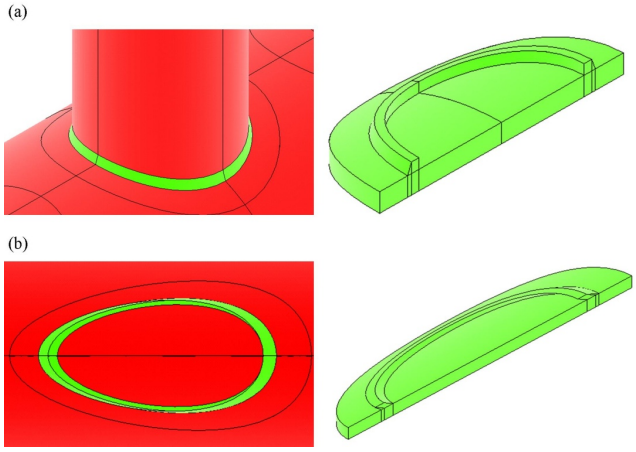

Fig. 5. Simulated weld profile: (a) Central brace, (b) Outer brace

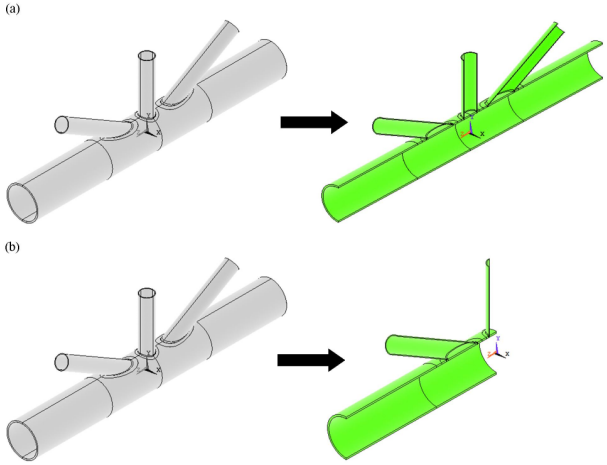

Fig. 6. Appropriate portion of the entire tubular KT-joint required to be modeled for each load case based on Table 1: (a) ½, (b) ¼

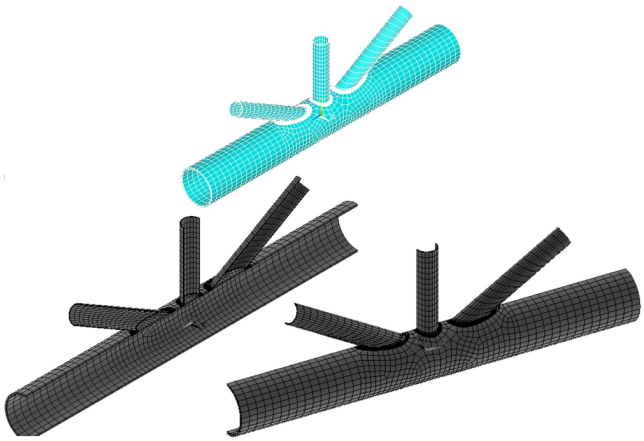

Fig. 7. Generated mesh for a tubular KT-joint using the sub-zone method

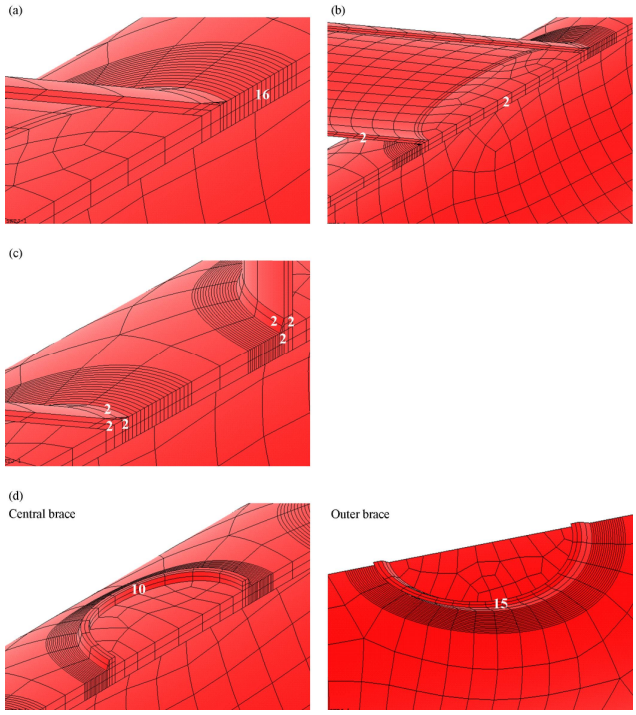

Fig. 8. The mesh density of: (a) Extrapolation region, (b) Chord and brace members, (c) Weld profile, (d) Brace-to-chord intersection

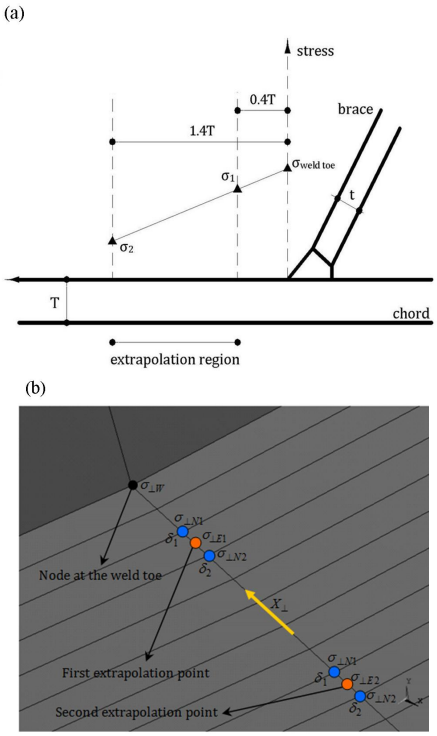

Fig. 9. (a) Extrapolation method recommended by IIW-XV-E [32], (b) Interpolations and extrapolations necessary to compute the DoB value based on the HSSs at the weld toe

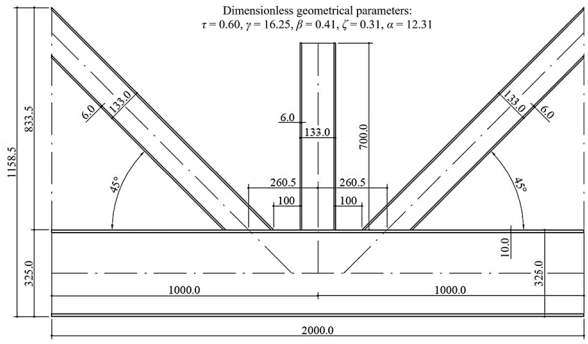

Fig. 10. Geometrical characteristics of tested tubular KT-joint specimen (unit: mm)

Fig. 11. Test setup: (a) View of the test rig and KT-joint specimen, (b) Strain gauges attached along the brace-to-chord intersection, (c) Connecting the strain gauges to the data logger

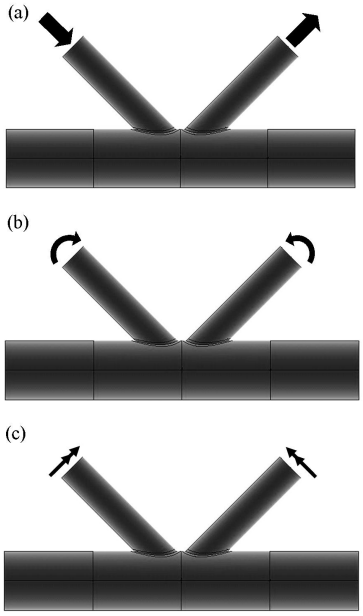

Fig. 12. Load cases for FE model validation: (a) Balanced axial loading studied by Morgan and Lee [3], (b) Balanced IPB loading studied by Ahmadi et al. [7], (c) Balanced OPB loading studied by Ahmadi and Asoodeh [8]

3.2. Details of parametric study

Altogether, 243 stress analyses were carried out on 81 FE models using ANSYS Ver. 11 to investigate the effects of dimensionless geometrical parameters on the DoB values at the saddle positions of the central and outer braces in tubular KT-joints subjected to three different types of OPB moment loading (Fig. 3).

Different values assigned to the parameters β, γ, τ, and θ have been presented in Table 5. These values cover the practical ranges of the dimensionless parameters typically found in tubular joints of offshore jacket structures. Providing that the gap between the braces is not very large, the relative gap ($\zeta = g / D$) has no considerable effect on stress and strain distribution. The validity range for this statement is $0.2 \leq \zeta \leq 0.6$ [19]. Hence, a typical value of $\zeta = 0.3$ was designated for all joints. Sufficiently long chord greater than six chord diameters (i.e. $\alpha \geq 12$) should be used to ensure that the stresses at the brace/chord intersection are not affected by the chord's boundary conditions [13]. The brace length has no effect on the HSSs when the parameter α_B is greater than critical value [16]. According to Chang and Dover [35], this critical value is about 6. In the present study, to avoid the effect of short brace length, a realistic value of α_B = 8 was selected for all joints.

The 81 generated models span the following ranges of geometrical parameters:

$$\begin{aligned} &0.4 \leq \beta \leq 0.6 \\ &12 \leq \gamma \leq 24 \\ &0.4 \leq \tau \leq 1.0 \\ &30^\circ \leq \theta \leq 60^\circ \end{aligned} \qquad (12)$$

3.3. Organization of the DoB samples

The DoB values extracted from the results of 243 FE analyses were organized as six samples for further statistical and probabilistic analyses. Samples 1−3 included the DoB values at the saddle position of the central brace under the 1st–3rd OPB loading conditions, respectively; while samples 4−6 included the DoB values at the saddle position of the outer brace under the 1st–3rd OPB loading conditions, respectively. Values of the size (n), mean (μ), standard deviation (σ), coefficient of skewness (α_3), and coefficient of kurtosis (α_4) for these samples are listed in Table 6.

The value of α_3 for the sample 4, that included the outer-brace DoB values under the 1st OPB load case, is positive which means that the probability distribution for this sample is expected to have a longer tail on the right, which is toward increasing values, than on the left. However, the value of α_3 for the other samples is negative meaning that the probability distribution for these samples is expected to have a longer tail on the left, which is toward decreasing values, than on the right.

The value of α_4 for the sample 5, that included the outer-brace DoB values under the 2nd OPB load case, is greater than three meaning that the probability distribution is expected to be sharp-peak (leptokurtic) for this sample; while the value of α_4 for the other DoB samples is smaller than three which means that for these samples, the probability distribution is expected to be mild-peak (platykurtic).

4. Application of the Freedman-Diaconis rule to generate the density histograms

To generate a density histogram, the range of data (R) is divided into several classes and the number of occurrences in each class is counted and tabulated. These are called frequencies. Then, the relative frequency of each class can be obtained through dividing its frequency by the sample size. Afterwards, the density is calculated for each class through dividing the relative frequency by the class width. The width of classes is usually made equal to facilitate interpretation.

Care should be exercised in the choice of the number of classes (n_c). Too few will cause an omission of some important features of the data; too many will not give a clear overall picture because there may be high fluctuations in the frequencies. One of the widely accepted rules to determine the number of classes is the Freedman-Diaconis rule expressed as follows [36]:

$$n_c = \frac{R\left(n^{1/3}\right)}{2\left(\mathrm{IQR}\right)} \tag{13}$$

where R is the range of sample data, n is the sample size, and IQR is the interquartile range calculated as:

$$\mathrm{IQR} = Q_3 - Q_1 \tag{14}$$

where Q_1 is the lower quartile which is the median of the lower half of the data; and likewise, Q_3 is the upper quartile that is the median of the upper half of the data.

Density histograms of generated samples are shown in Fig. 13. This figure shows that, as it was expected from the values of α_3 and α_4 in Table 6, the right tail is longer than the left one in the histogram of sample 4; while in the histograms of other samples, the left tail is longer. Moreover, the histogram of sample 5 is leptokurtic, while the histograms of other samples are platykurtic

5. PDF fitting based on the ML method

Thirteen different PDFs were fitted to the density histograms to assess the degree of fitting of various distributions to the DoB samples. In each case, distribution parameters were estimated using the maximum likelihood (ML) method. Results are given in Table 7. The ML procedure is an alternative to the method of moments. As a means of finding an estimator, statisticians often give it preference. For a random variable X with a known PDF, $f_X(x)$, and observed values $x_1, x_2, \ldots, x_n$, in a random sample of size n, the likelihood function of ω, where ω represents the vector of unknown parameters, is defined as:

$$L(\omega) = \prod_{i=1}^{n} f_X\left(x_i \mid \omega\right) \tag{15}$$

The objective is to maximize $L(\omega)$ for the given data set. It is done by taking m partial derivatives of $L(\omega)$, where m is the number of parameters, and equating them to zero. Then the maximum likelihood estimators (MLEs) of the parameter set ω can be found from the solutions of equations. In this way the greatest probability is given to the observed set of events, provided that the true form of the probability distribution is known.

6. Assessing the goodness-of-fit based on the Kolmogorov-Smirnov test

The Kolmogorov-Smirnov goodness-of-fit test is a nonparametric test that relates to the cumulative distribution function (CDF) of a continuous variable. The test statistic, in a two-sided test, is the maximum absolute difference (which is usually the vertical distance) between the empirical and hypothetical CDFs. For a continuous variate X, let $x_{(1)}, x_{(2)}, \ldots, x_{(n)}$ represent the order statistics of a sample of the size n, that is, the values arranged in increasing order. The empirical or sample distribution function $F_n(x)$ is a step function. This gives the proportion of values not exceeding x and is defined as:

$$\begin{aligned} F_n(x) &= 0, && \text{For } x < x_{(1)} \\ &= k/n, && \text{For } x_{(k)} \le x < x_{(k+1)} \\ & && k = 1, 2, \ldots, n-1 \\ &= 1, && \text{For } x \ge x_{(n)} \end{aligned} \tag{16}$$

Empirical distribution functions for generated DoB samples have been shown in Fig. 14.

Let $F_0(x)$ denote a completely specified theoretical continuous CDF. The null hypothesis H_0 is that the true CDF of X is the same as $F_0(x)$. That is, under the null hypothesis:

$$\lim_{n\to\infty} \Pr\left[F_n(x) = F_0(x)\right] = 1 \tag{17}$$

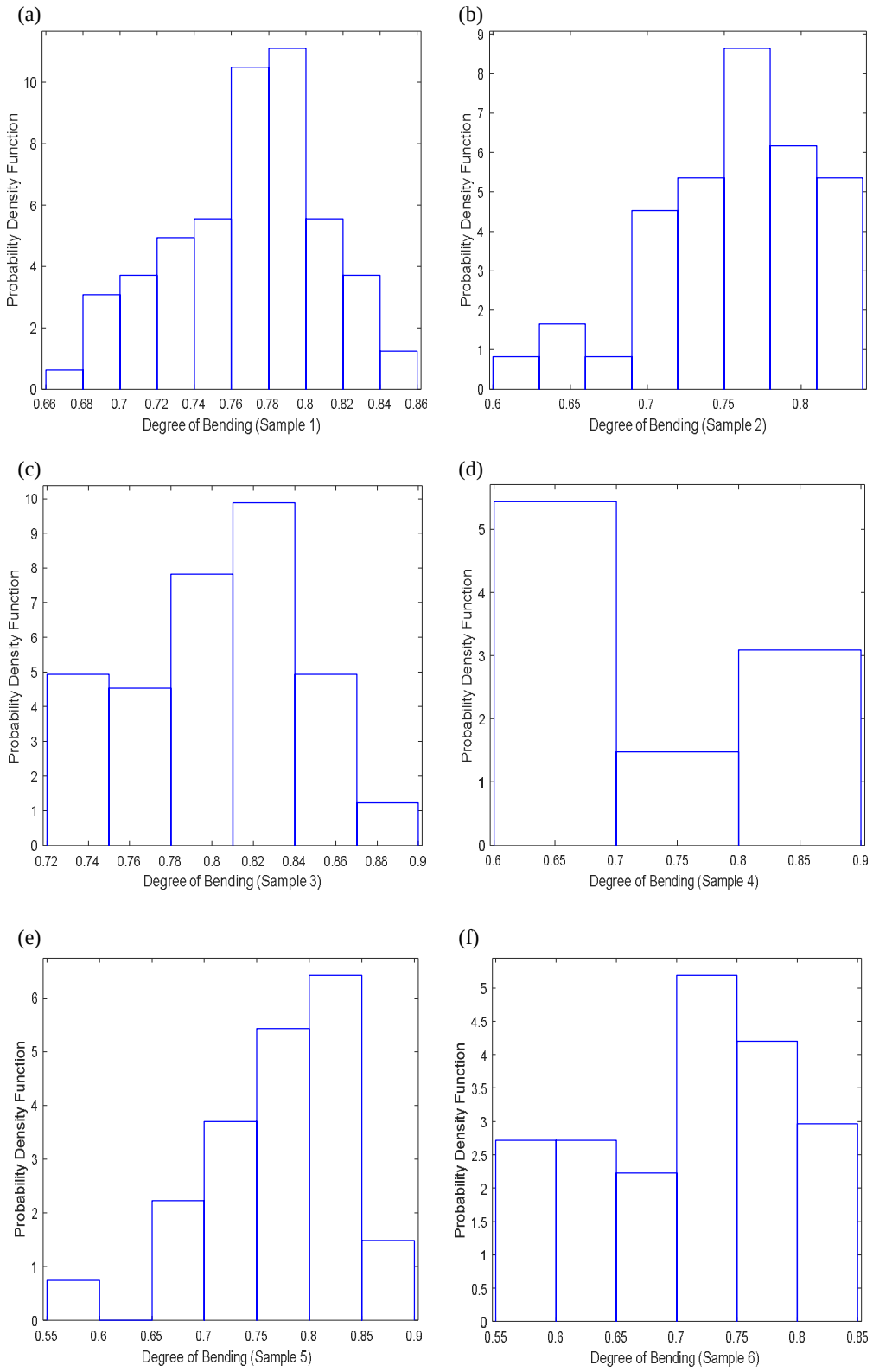

Fig. 13. Density histograms generated for the DoB samples: (a) Sample 1 (Saddle position of the central brace–1st OPB loading condition), (b) Sample 2 (Saddle position of the central brace–2nd OPB loading condition), (c) Sample 3 (Saddle position of the central brace–3rd OPB loading condition), (d) Sample 4 (Saddle position of the outer brace–1st OPB loading condition), (e) Sample 5 (Saddle position of the outer brace–2nd OPB loading condition), (f) Sample 6 (Saddle position of the outer brace–3rd OPB loading condition)

The test criterion is the maximum absolute difference between $F_n(x)$ and $F_0(x)$, formally defined as:

$$d_n = \sup_x \left| F_n(x) - F_0(x) \right| \tag{18}$$

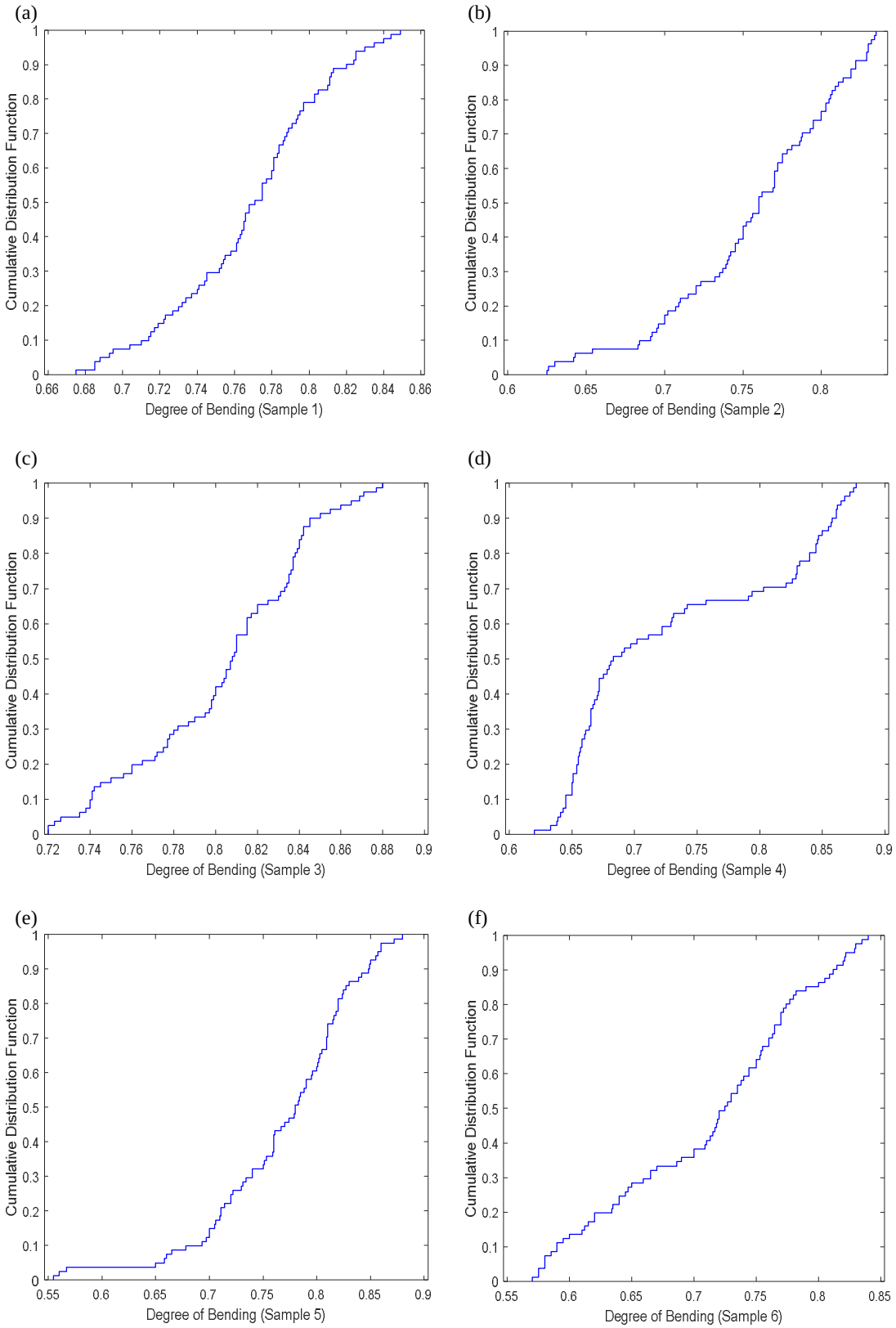

Fig. 14. Empirical cumulative distribution functions for generated DoB samples: (a) Sample 1 (Saddle position of the central brace−1st OPB loading condition), (b) Sample 2 (Saddle position of the central brace−2nd OPB loading condition), (c) Sample 3 (Saddle position of the central brace−3rd OPB loading condition), (d) Sample 4 (Saddle position of the outer brace−1st OPB loading condition), (e) Sample 5 (Saddle position of the outer brace−2nd OPB loading condition), (f) Sample 6 (Saddle position of the outer brace−3rd OPB loading condition)

Theoretical continuous CDFs fitted to the empirical distribution functions of generated DoB samples have been shown in Fig. 15.

A large value of this statistic (d_n) indicates poor fit. Hence, acceptable values should be known. The critical values $D_{n,\xi}$ for large samples, say $n > 35$, are $(1.3581/\sqrt{n})$ and $(1.6276/\sqrt{n})$ for $\xi = 0.05$ and 0.01, respectively [36] where ξ is the significance level.

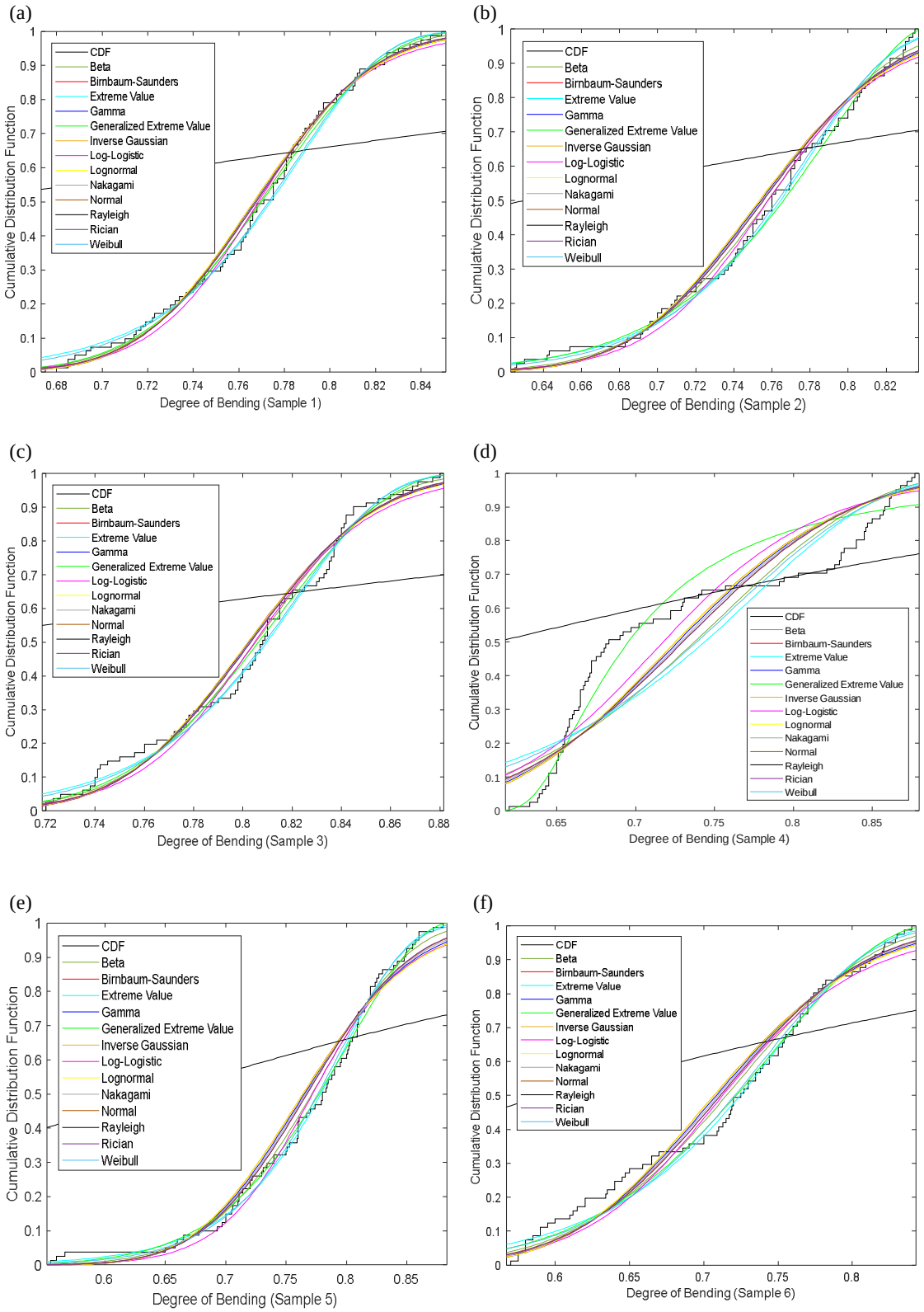

Fig. 15. Theoretical continuous CDFs fitted to the empirical CDFs of generated DoB samples: (a) Sample 1 (Saddle position of the central brace−1st OPB loading condition), (b) Sample 2 (Saddle position of the central brace−2nd OPB loading condition), (c) Sample 3 (Saddle position of the central brace−3rd OPB loading condition), (d) Sample 4 (Saddle position of the outer brace−1st OPB loading condition), (e) Sample 5 (Saddle position of the outer brace−2nd OPB loading condition), (f) Sample 6 (Saddle position of the outer brace−3rd OPB loading condition)

Results of the Kolmogorov-Smirnov test for the six prepared samples are given in Tables 8−13. It is evident in these tables that the Weibull distribution has the smallest d_n value for samples 2, 3, and 5; while the Beta distribution has the smallest d_n for samples 1 and 6; and the Generalized Extreme Value distribution has the smallest d_n value for sample 4. Hence, they are the best-fitted distributions for the corresponding DoB samples (Fig. 16).

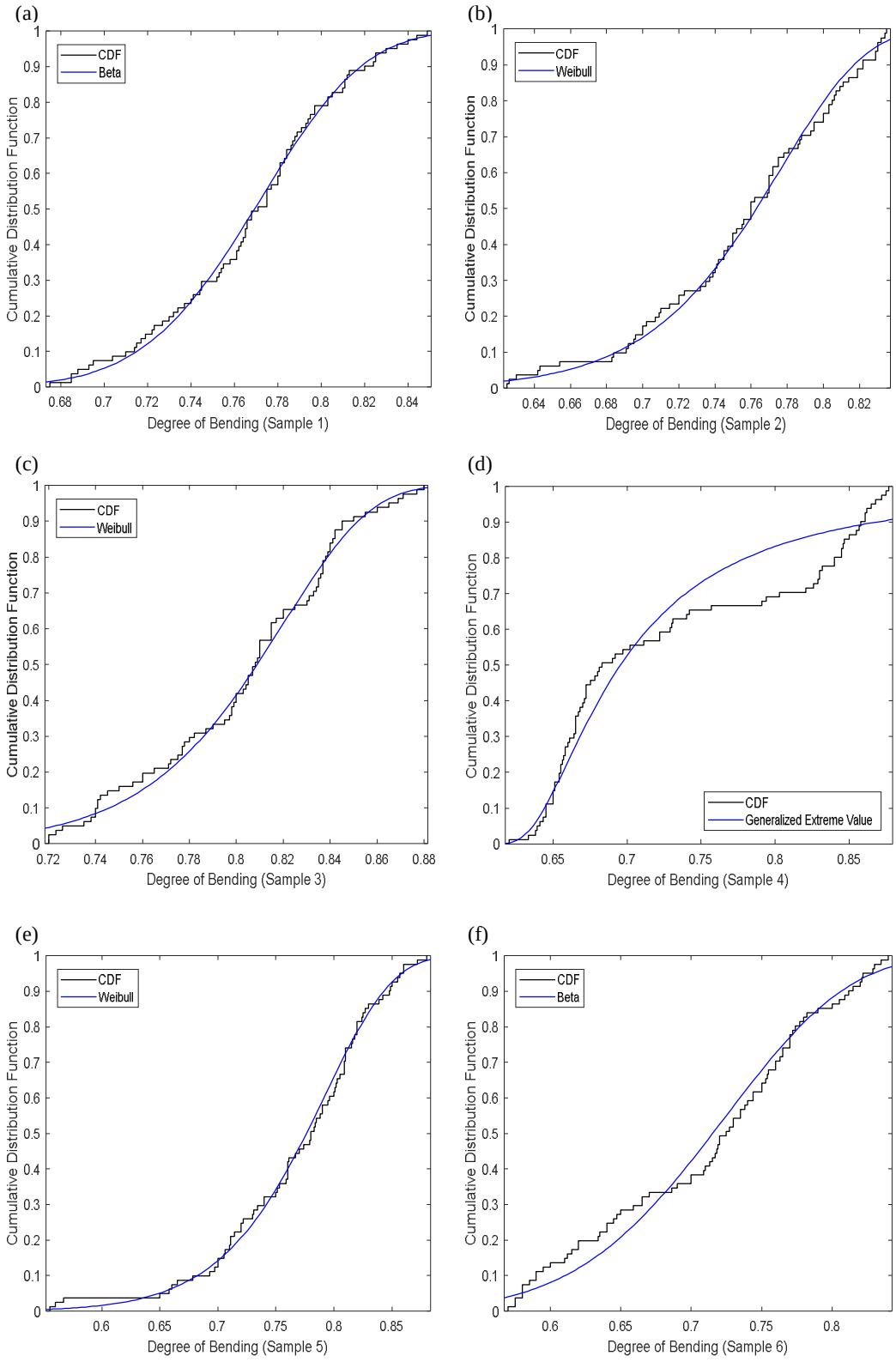

Fig. 16. The best-fitted distributions according to the Kolmogorov-Smirnov test: (a) Sample 1 (Saddle position of the central brace−1st OPB loading condition), (b) Sample 2 (Saddle position of the central brace−2nd OPB loading condition), (c) Sample 3 (Saddle position of the central brace−3rd OPB loading condition), (d) Sample 4 (Saddle position of the outer brace−1st OPB loading condition), (e) Sample 5 (Saddle position of the outer brace−2nd OPB loading condition), (f) Sample 6 (Saddle position of the outer brace−3rd OPB loading condition)

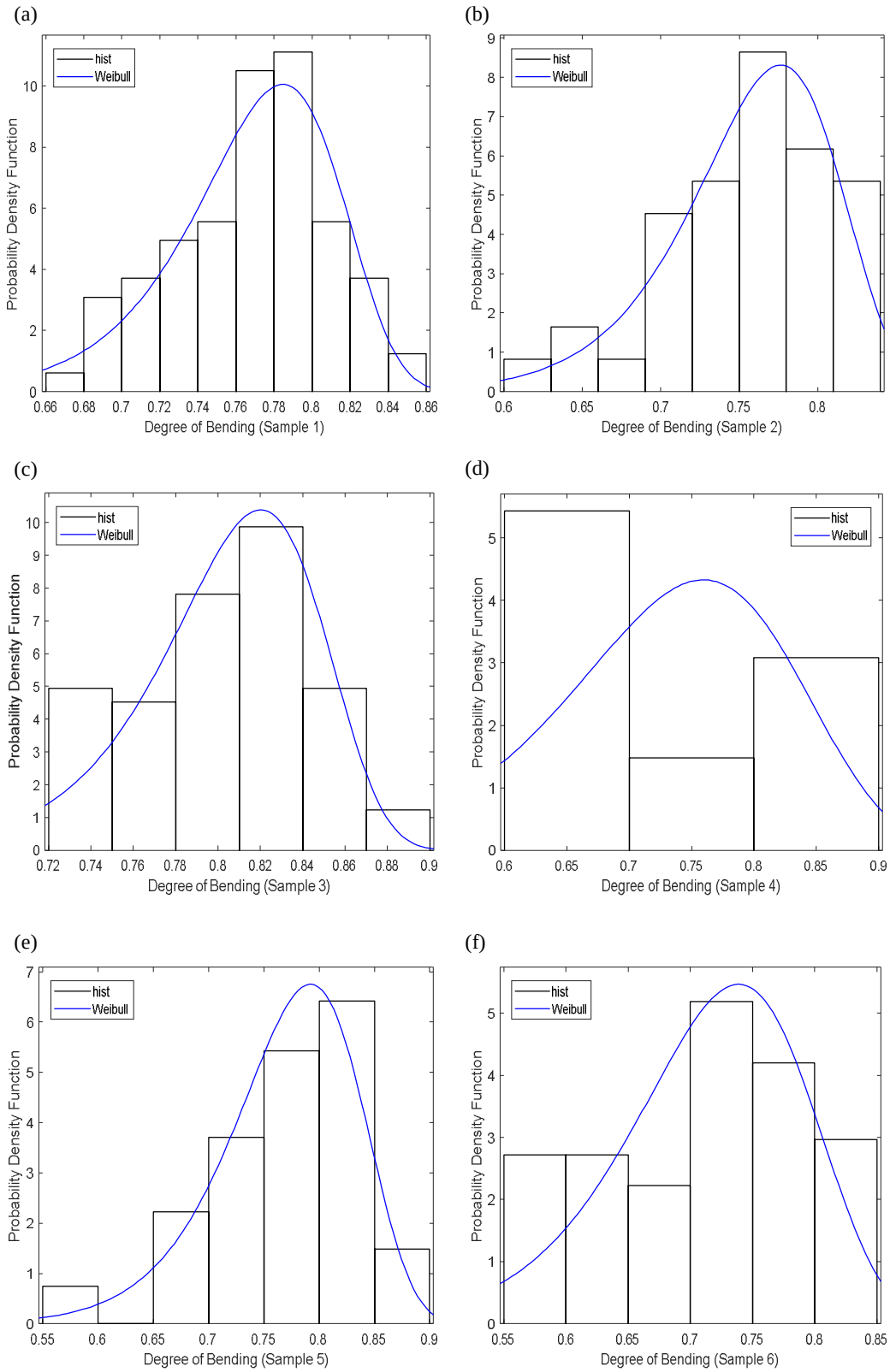

Fig. 17. Proposed PDFs for generated DoB samples: (a) Sample 1 (Saddle position of the central brace−1st OPB loading condition), (b) Sample 2 (Saddle position of the central brace−2nd OPB loading condition), (c) Sample 3 (Saddle position of the central brace−3rd OPB loading condition), (d) Sample 4 (Saddle position of the outer brace−1st OPB loading condition), (e) Sample 5 (Saddle position of the outer brace−2nd OPB loading condition), (f) Sample 6 (Saddle position of the outer brace−3rd OPB loading condition)

7. Proposed probability distribution model for the DoB

The best-fitted distributions for the generated DoB samples were introduced in Sect. 6. According to the results of the Kolmogorov-Smirnov test, the best-fitted distributions for the six samples studied include three different models: Weibull, Beta, and Generalized Extreme Value distributions. Results of the test for sample 1 are given in Table 8 as an example. The

diversity of the best-fitted probability models derived for the studied DoB values may practically result in the confusion and difficulty of their application for the fatigue reliability analysis and design. Hence, reducing the number of distribution types proposed for the DoB values might be a good idea. To do so, the top three distribution functions for each DoB sample were identified (Table 9). The aim was to propose a single probability model to cover all the DoB samples.

Table 7. Estimated parameters for PDFs fitted to the density histograms of DoB samples at the saddle positions of central and outer braces under the OPB loadings

Fitted PDF	Parameters	Estimated values					
		Sample 1	Sample 2	Sample 3	Sample 4	Sample 5	Sample 6
		Central brace, 1st OPB LC	Central brace, 2nd OPB LC	Central brace, 3rd OPB LC	Outer brace, 1st OPB LC	Outer brace, 2nd OPB LC	Outer brace, 3rd OPB LC
Beta	a	83.8823	50.743	78.3375	17.5857	31.1492	24.5695
	b	25.3897	16.4367	19.2069	6.47731	9.46798	9.97889
Birnbaum-Saunders	β_0	0.766573	0.753467	0.802076	0.725243	0.763867	0.706875
	γ_0	0.0531083	0.0722212	0.0508064	0.114098	0.0940614	0.111056
Extreme Value	μ	0.787314	0.780396	0.822556	0.774508	0.798101	0.748376
	σ	0.0364656	0.0433962	0.0351623	0.0841897	0.0530766	0.0656653
Gamma	a	357.355	195.681	390.627	75.8396	118.292	82.8304
	b	0.00214815	0.00386053	0.00205595	0.00962509	0.00648605	0.00858664
Generalized Extreme Value	k	-0.391922	-0.646434	-0.435386	0.481081	-0.559969	-0.531689
	σ	0.042301	0.0598337	0.0428433	0.0472531	0.0737407	0.0840801
	μ	0.755539	0.746487	0.791866	0.676441	0.752732	0.693635
Inverse Gaussian	μ	0.767654	0.755432	0.803111	0.729963	0.767247	0.711235
	λ	271.979	144.644	310.928	55.8902	86.5272	57.4896
Log-logistic	μ	-0.263184	-0.277077	-0.217255	-0.332146	-0.259053	-0.338664
	σ	0.0305197	0.0408412	0.0295985	0.069967	0.0499815	0.0659058
Lognormal	μ	-0.265816	-0.283023	-0.220543	-0.321369	-0.269179	-0.346802
	σ	0.0534228	0.0726227	0.05111	0.114712	0.0944668	0.111631
Nakagami	μ	90.0914	49.9548	98.5318	18.8403	30.8618	21.232
	ω	0.590922	0.573497	0.646616	0.54012	0.593291	0.511776
Normal	μ	0.767654	0.755432	0.803111	0.729963	0.767247	0.711235
	σ	0.0406125	0.0534259	0.0406088	0.0858191	0.0684187	0.0774278
Rayleigh	b	0.543563	0.535489	0.568602	0.519673	0.544652	0.505854
Rician	s	0.76659	0.753555	0.802094	0.724892	0.764204	0.707009
	σ	0.0403892	0.0531614	0.040383	0.0855907	0.0681317	0.0771814
Weibull	a	0.786417	0.779049	0.821756	0.76943	0.796071	0.745173
	b	21.4633	17.5732	23.183	8.99524	14.5745	11.0243

Table 8. Results of the Kolmogorov-Smirnov goodness-of-fit test for DoB sample 1 (Central brace−1st OPB LC)

Fitted distribution	Test statistic (d_n)	Critical value ($D_{n,\xi}$)		Test result	
		$\xi = 0.05$	$\xi = 0.01$	$\xi = 0.05$	$\xi = 0.01$
Beta	0.037064			Accept	Accept
Birnbaum-Saunders	0.062642			Accept	Accept
Extreme Value	0.067938			Accept	Accept
Gamma	0.058971			Accept	Accept
Generalized Extreme Value	0.042086			Accept	Accept
Inverse Gaussian	0.062647			Accept	Accept
Log-logistic	0.054059	0.1509	0.180844444	Accept	Accept
Lognormal	0.062892			Accept	Accept
Nakagami	0.05544			Accept	Accept
Normal	0.052209			Accept	Accept
Rayleigh	0.537469			Reject	Reject
Rician	0.051817			Accept	Accept
Weibull	0.058837			Accept	Accept

Table 9. Best-fitted distributions for the DoB samples at the saddle positions of the central and outer braces based on the results of the Kolmogorov-Smirnov test

Best-fitted distributions	DoB samples					
	Sample 1 Central brace, 1st OPB LC	Sample 2 Central brace, 2nd OPB LC	Sample 3 Central brace, 3rd OPB LC	Sample 4 Outer brace, 1st OPB LC	Sample 5 Outer brace, 2nd OPB LC	Sample 6 Outer brace, 3rd OPB LC
#1	Beta	Weibull	Weibull	Generalized Extreme Value	Weibull	Beta
#2	Generalized Extreme Value	Beta	Generalized Extreme Value	-	Extreme Value	Generalized Extreme Value
#3	Rician	Extreme Value	Extreme Value	-	Generalized Extreme Value	Extreme Value

Table 10. Comparison of the test statistics for the proposed and the best-fitted distributions based on the results of the Kolmogorov-Smirnov test

	Test statistic					
	Sample 1 Central brace, 1st OPB LC	Sample 2 Central brace, 2nd OPB LC	Sample 3 Central brace, 3rd OPB LC	Sample 4 Outer brace, 1st OPB LC	Sample 5 Outer brace, 2nd OPB LC	Sample 6 Outer brace, 3rd OPB LC
Best-fitted distribution	0.037064 (Beta)	0.044443 (Weibull)	0.056591 (Weibull)	0.142567 (Generalized Extreme Value)	0.045182 (Weibull)	0.076427 (Beta)
Proposed distribution	0.058837 (Weibull)	0.044443 (Weibull)	0.056591 (Weibull)	- (Weibull)	0.045182 (Weibull)	0.0851 (Weibull)
Difference	58.74%	0%	0%	-	0%	11.35%

After surveying the data presented in Table 9, the Weibull model is proposed as the governing probability distribution function for DoB values. The difference between the test statistics of the proposed distribution and the best-fitted one for each sample is presented in Table 10. Using the information presented in these tables, the analyst can make a choice, based on the engineering judgment, between the best-fitted and the proposed probability models for each of the studied cases.

The PDF of Weibull distribution is expressed as:

$$f_X(x|a,b) = \frac{b}{a}\left(\frac{x}{a}\right)^{b-1} e^{-(x/a)^b} \quad (19)$$

After substituting the values of estimated parameters from Table 7, following probability density functions are proposed for the DoB values in tubular KT-joints subjected to the three considered OPB load cases defined in Fig. 3:

Saddle position of the central brace−1st load case:

$$f_X(x) = 27.292\left(\frac{x}{0.7864}\right)^{20.463} e^{-(x/0.7864)^{21.463}} \quad (20)$$

Saddle position of the central brace−2nd load case:

$$f_X(x) = 22.557\left(\frac{x}{0.7791}\right)^{16.573} e^{-(x/0.7791)^{17.573}} \quad (21)$$

Saddle position of the central brace−3rd load case:

$$f_X(x) = 28.211\left(\frac{x}{0.8218}\right)^{22.183} e^{-(x/0.8218)^{23.183}} \quad (22)$$

Saddle position of the outer brace−1st load case:

$$f_X(x) = 11.691\left(\frac{x}{0.7694}\right)^{7.9952} e^{-(x/0.7694)^{8.9952}} \quad (23)$$

Saddle position of the outer brace−2nd load case:

$$f_X(x) = 18.308\left(\frac{x}{0.7961}\right)^{13.574} e^{-(x/0.7961)^{14.575}} \quad (24)$$

Saddle position of the outer brace−3rd load case:

$$f_X(x) = 14.794\left(\frac{x}{0.7452}\right)^{10.024} e^{-(x/0.7452)^{11.024}} \quad (25)$$

where X denotes the DoB as a random variable and x represents its values.

Developed PDFs, shown in Fig. 17, can be adapted in the fatigue reliability analysis and design of OPB-loaded tubular KT-joints commonly found in offshore jacket structures.

8. Conclusions

A total of 243 FE analyses were carried out in the present research on 81 models of KT-joints subjected to three types of OPB moment loading. Generated FE models were validated using experimental data, previous FE results, and available parametric equations. FE analysis results were used to develop a set of PDFs for the DoB in OPB-loaded KT-joints. Based on the results of parametric FE study, a sample database was prepared for the DoB values and density histograms were generated for respective samples

based on the Freedman-Diaconis rule. Thirteen theoretical PDFs were fitted to the developed histograms, and the ML method was applied to evaluate the parameters of fitted PDFs. In each case, the Kolmogorov-Smirnov test was used to evaluate the goodness of fit. Finally, the Weibull model was proposed as the governing probability distribution function for the DoB. After substituting the values of estimated parameters, six fully defined PDFs were presented for the DoB at the saddle positions of the central and outer braces in tubular KT-joints subjected to three types of OPB moment loading.

References

[1] Connolly MPM. A fracture mechanics approach to the fatigue assessment of tubular welded Y and K-joints. PhD Thesis, University College London, UK; 1986.

[2] Chang E, Dover WD. Prediction of degree of bending in tubular X and DT joints. International Journal of Fatigue 1999;21(2):147–61.

[3] Morgan MR, Lee MMK. Prediction of stress concentrations and degrees of bending in axially loaded tubular K-joints. Journal of Constructional Steel Research 1998;45(1):67–97.

[4] UK Department of Energy (DoE). Background to new fatigue design guidance for steel joints and connections in offshore structures. London, UK; 1995.

[5] Lee MMK, Bowness D. Estimation of stress intensity factor solutions for weld toe cracks in offshore tubular joints. International Journal of Fatigue 2002;24:861–75.

[6] Shen W, Choo YS. Stress intensity factor for a tubular T-joint with grouted chord. Engineering Structures 2012;35:37–47.

[7] Ahmadi H, Lotfollahi-Yaghin MA, Asoodeh Sh. Degree of bending (DoB) in tubular K-joints of offshore structures subjected to in-plane bending (IPB) loads: Study of geometrical effects and parametric formulation. Ocean Engineering 2015;102:105–16.

[8] Ahmadi H, Asoodeh Sh. Parametric study of geometrical effects on the degree of bending (DoB) in offshore tubular K-joints under out-of-plane bending loads. Applied Ocean Research 2016;58:1–10.

[9] Ahmadi H, Asoodeh Sh. Degree of bending (DoB) in tubular KT-joints of jacket structures subjected to axial loads. International Journal of Maritime Technology 2015;4(2):65–75.

[10] Ahmadi H, Amini Niaki M. Effects of geometrical parameters on the degree of bending (DoB) in two-planar tubular DT-joints of offshore jacket structures subjected to axial and bending loads. Marine Structures 2019;64(C):229−245.

[11] Ahmadi H, Ghaffari AR. Probabilistic assessment of degree of bending (DoB) in tubular X-joints of offshore structures subjected to bending loads. Advances in Civil Engineering 2015;1–12.

[12] Ahmadi H, Ghaffari AR. Probabilistic analysis of stress intensity factor (SIF) and degree of bending (DoB) in axially loaded tubular K-joints of offshore structures. Latin American Journal of Solids and Structures 2015;12(11):2025–2044.

[13] Efthymiou M. Development of SCF formulae and generalized influence functions for use in fatigue analysis. OTJ 88, Surrey, UK; 1988.

[14] Hellier AK, Connolly M, Dover WD. Stress concentration factors for tubular Y and T-joints. International Journal of Fatigue 1990;12:13–23.

[15] Morgan MR, Lee MMK. Parametric equations for distributions of stress concentration factors in tubular K-joints under out-of-plane moment loading. International Journal of Fatigue 1998;20:449–61.

[16] Chang E, Dover WD. Parametric equations to predict stress distributions along the intersection of tubular X and DT-joints. International Journal of Fatigue 1999;21:619–35.

[17] Shao YB. Geometrical effect on the stress distribution along weld toe for tubular T- and K-joints under axial loading. Journal of Constructional Steel Research 2007;63:1351–60.

[18] Shao YB, Du ZF, Lie ST. Prediction of hot spot stress distribution for tubular K-joints under basic loadings. Journal of Constructional Steel Research 2009;65:2011–26.

[19] Lotfollahi-Yaghin MA, Ahmadi H. Effect of geometrical parameters on SCF distribution along the weld toe of tubular KT-joints under balanced axial loads. International Journal of Fatigue 2010;32:703–19.

[20] Ahmadi H, Lotfollahi-Yaghin MA, Aminfar MH. Geometrical effect on SCF distribution in uni-planar tubular DKT-joints under axial loads. Journal of Constructional Steel Research 2011;67:1282–91.

[21] Lotfollahi-Yaghin MA, Ahmadi H. Geometric stress distribution along the weld toe of the outer brace in two-planar tubular DKT-joints: parametric study and deriving the SCF design equations. Marine Structures 2011;24:239–60.

[22] Ahmadi H, Lotfollahi-Yaghin MA. Geometrically parametric study of central brace SCFs in offshore three-planar tubular KT-joints. Journal of Constructional Steel Research 2012;71:149–61.

[23] Ahmadi H, Lotfollahi-Yaghin MA, Shao YB. Chord-side SCF distribution of central brace in internally ring-stiffened tubular KT-joints: A geometrically parametric study. Thin-Walled Structures 2013;70:93−105.

[24] Ahmadi H, Zavvar E. The effect of multi-planarity on the SCFs in offshore tubular KT-joints subjected to in-plane and out-of-plane bending loads. Thin-Walled Structures 2016;106:148−165.

[25] Shao YB, Lie ST. Parametric equation of stress intensity factor for tubular K-joint under balanced axial loads. International Journal of Fatigue 2005;27:666–79.

[26] Shao YB. Analysis of stress intensity factor (SIF) for cracked tubular K-joints subjected to balanced axial load. Engineering Failure Analysis 2006;13:44–64.

[27] American Welding Society (AWS). Structural welding code: AWS D 1.1. Miami (FL), US; 2002.

[28] Lie ST, Lee CK, Wong SM. Modeling and mesh generation of weld profile in tubular Y-joint. Journal of Constructional Steel Research 2001;57:547–67.

[29] Ahmadi H, Lotfollahi-Yaghin MA, Shao YB, Aminfar MH. Parametric study and formulation of outer-brace geometric stress concentration factors in internally ring-stiffened tubular KT-joints of offshore structures. Applied Ocean Research 2012;38:74–91.

[30] Wordsworth AC, Smedley GP. Stress concentrations at unstiffened tubular joints. Proceedings of the European Offshore Steels Research Seminar, Paper 31, Cambridge, UK; 1978.

[31] Smedley P, Fisher P. Stress concentration factors for simple tubular joints. Proceedings of the International Offshore and Polar Engineering Conference (ISOPE), Edinburgh; 1991. p. 475–83.

[32] IIW-XV-E. Recommended fatigue design procedure for welded hollow section joints, IIW Docs, XV-1035-99/XIII-1804-99. International Institute of Welding, France; 1999.

[33] Ahmadi H. Experimental and numerical investigation of the SCF distribution in unstiffened and stiffened uniplanar tubular KT-joints of steel platforms and the extension of numerical study to multi-planar joints. PhD Thesis, Faculty of Civil Engineering, University of Tabriz, Tabriz, Iran; 2012 (In Farsi).

[34] UK Health and Safety Executive. OTH 354: Stress concentration factors for simple tubular joints-assessment of existing and development of new parametric formulae. Prepared by Lloyd's Register of Shipping, UK, 1997.

[35] Chang E, Dover WD. Stress concentration factor parametric equations for tubular X and DT joints. International Journal of Fatigue 1996;18(6):363–87.

[36] Kottegoda NT, Rosso R. Applied statistics for civil and environmental engineers. 2nd Edition, Blackwell Publishing Ltd, UK; 2008.